Showcasing artwork by Associate Professor Guoping Yang and Professor Yunhai Liu from School of Chemistry and Materials Science, Jiangxi Key Laboratory for Mass Spectrometry and Instrumentation, East China University of Technology, China, and Professor Yongge Wei *et al.* from Department of Chemistry, Tsinghua University, China.

Highly-stable Silverton-type U^{IV}-containing polyoxomolybdate frameworks for the heterogeneous catalytic synthesis of quinazolinones

The first series of Silverton-type $\{U^{IV}Mo_{12}O_{40}\}$-based polyoxomolybdates with 3D frameworks linked by transitional metal ions were synthesized and characterized, which exhibit excellent solvent and pH stabilities and can be used as heterogeneous catalysts for the catalytic synthesis of quinazolinone drug precursor skeletons in high yields and selectivity.

Credit: artist Ms Qinqin Wei and Quinn Studio.

As featured in:

See Guoping Yang, Yunhai Liu, Yongge Wei *et al.*, *Green Chem.*, 2024, **26**, 6454.

ROYAL SOCIETY OF CHEMISTRY

rsc.li/greenchem

Registered charity number: 207890

Green Chemistry

PAPER

View Article Online
View Journal | View Issue

Cite this: *Green Chem.*, 2024, **26**, 6454

Highly-stable Silverton-type U^{IV}-containing polyoxomolybdate frameworks for the heterogeneous catalytic synthesis of quinazolinones†

Ke Li,‡[a] Yufeng Liu,‡[a] Guoping Yang, *[a,c] Zhijian Zheng, [a] Xiaoling Lin,[a] Zhibin Zhang,[a] Shujun Li, [b] Yunhai Liu*[a] and Yongge Wei *[c]

Received 21st February 2024,
Accepted 1st April 2024

DOI: 10.1039/d4gc00877d

rsc.li/greenchem

Heteroatoms are very important in polyoxometalates (POMs) because they can lead to appealing architectures and unexpected properties in the final POMs. In this work, we elaborately designed and isolated three Silverton-type POMs ($[U^{IV}Mo_{12}O_{42}]^{8-}$) with U^{IV} as the heteroatom and linked by Fe^{II} (**FeUMo**), Co^{II} (**CoUMo**) and Ni^{II} (**NiUMo**). These Silverton-type U-containing polyoxomolybdates were demonstrated to be the first molecular catalysts for the synthesis of quinazolinone drug precursor skeletons. Under the optimized reaction conditions, 27 quinazolinones could be obtained in high yield with water as the sole by-product under mild conditions. Furthermore, **NiUMo** can be recycled seven times and still keep high stability and catalytic activity.

Introduction

Nuclear power stands out as an efficient and reliable emerging energy source, representing a pivotal technology that is well-equipped to address the escalating energy demand.[1–3] Uranium serves as the primary fuel for nuclear reactors and constitutes the principal component of nuclear waste, presenting significant potential for advancements in environmental safety.[4,5] Therefore, studying the solution and solid-state chemistry of uranium is imperative for the implementation of the nuclear fuel cycle, as well as monitoring contamination in the environment and treating nuclear wastes.[6–12] POMs are a class of inorganic metal–oxygen clusters built from the connection of $\{MO_x\}$ polyhedra (M = V, Nb, Mo, or W, *etc.*, x = 5, 6).[13–18] They are good candidates to attract and uptake uranium or uranyl ions based on the strong electrostatic interactions between POMs and uranium or uranyl ions.[19–21] The resulting uranium-containing POMs (U-POMs) can serve as molecular models for understanding the behavior of actinides in laboratories and environmental systems and have potential applications in separating actinides from complex solutions based on size or mass.[22,23]

U-POMs have been studied since the early 1970s,[24] and dozens of Keggin-type U-POMs, several Dawson-type, and other type structures were reported.[21,25,26] Generally, UO_2^{2+} and U^{4+} ions in the reported structures act as links or insertion atoms sandwiched by POM moieties, while U^{4+} ions can be used as heteroatoms only in Silverton-type U-POMs. From 1981 to 1990, Torchenkova and co-workers reported nine Silverton-type $\{UMo_{12}\}$-based structures, most of which are 0D structures.[21,27–35] Uranium with a particular valence state and action in the Silverton-type U-POMs can provide the opportunity for understanding the solution and solid-state chemistry of uranium, and its potential applications in actinide separation.[22,23,36] However, it can be easily recognized from the previous work that the research on Silverton-type U-POMs is very superficial. Thus, the study of their properties is a blank field to be developed.

Concerning the foregoing, we successfully designed and synthesized three Silverton-type multidimensional U-POMs connected by transition metal (TM) ions, *i.e.*, $Na_3H_3(H_2O)_9[FeUMo_{12}O_{42}]\cdot 4.5H_2O$ (**FeUMo**), $Na_{3.6}H_{2.4}(H_2O)_9[CoUMo_{12}O_{42}]\cdot 4.5H_2O$ (**CoUMo**), and $Na_{3.3}H_{2.7}(H_2O)_9[Ni_{0.58}UMo_{12}O_{42}]\cdot 4.5H_2O$ (**NiUMo**), which are the first series of U-POMs connected by TM

[a]*School of Chemistry and Materials Science, Jiangxi Key Laboratory for Mass Spectrometry and Instrumentation, East China University of Technology, Nanchang, Jiangxi 330013, China. E-mail: erick@ecut.edu.cn, yhliu@ecut.edu.cn*
[b]*School of Chemistry and Chemical Engineering, Henan Key Laboratory of Boron Chemistry and Advanced Energy Materials, Henan Normal University, Xinxiang, Henan 453007, China*
[c]*Key Lab of Organic Optoelectronics & Molecular Engineering of Ministry of Education, Department of Chemistry, Tsinghua University, Beijing 100084, China. E-mail: yonggewei@mail.tsinghua.edu.cn*

†Electronic supplementary information (ESI) available: Crystal information files (CIF), BVS, FT-IR, Raman, PXRD, TGA, condition screening, NMR and experimental details. CCDC 2222603, 2222722, 2222723 and 2292524. For ESI and crystallographic data in CIF or other electronic format see DOI: https://doi.org/10.1039/d4gc00877d

‡Contributed equally to this work.

ions with hetero-atoms of U^{IV}. These compounds crystallized in aqueous solutions containing TM ions may provide a research idea candidate for the study of the different crystallization behaviors of uranium and transition metals. The ordered and closely-packed multidimensional structures of these compounds would provide nanoscale control of the composition as precursors in the manufacturing of novel nuclear fuels and waste forms. Furthermore, as pure inorganic POMs, the title compounds exhibit outstanding stability and were used for the first time as molecular catalysts for the synthesis of quinazolinone drug precursor skeletons.

Results and discussion

Structural analysis and characterization of FeUMo, CoUMo, and NiUMo

The single-crystal X-ray diffraction analysis reveals that the polyanions in **FeUMo**, **CoUMo**, and **NiUMo** are similar and show the typical Silverton-type $\{UMo_{12}O_{42}\}$ structure (Fig. 1a). Furthermore, the frameworks of **FeUMo**, **CoUMo**, and **NiUMo** are isomorphic (Fig. S1–S3†). Both of them have a one-dimensional chain structure with the formula of $\{XUMo_{12}\}_n$ (X = Fe, Co, and Ni). Thus, only the structure of **FeUMo** is discussed in detail here. **FeUMo** crystallized in the $Ia\bar{3}$ space group (No. 206) from the cubic crystal system (Table S1†). Due to the high symmetry, the asymmetric unit of **FeUMo** is only 1/6 of the whole structure and consists of two 1/6 U^{IV} (U1 and U2), one 1/3 Fe^{II} (Fe1), four Mo^{VI} (Mo1–Mo4), two disordered Na ions, fourteen oxygen atoms (O1–O14) from the $\{UMo_{12}\}$ units, three coordination, and one and a half lattice water molecules (Fig. S1†). The 12-coordinated U1 and U2 ions in the center of the Silverton-type $\{UMo_{12}O_{42}\}$ polyanion are in the typical +4 valence. Due to the high symmetry, there are only two types of U–O bonds for each U center, namely six equivalent U1–O5, U1–O8, U2–O13, and U2–O14 bonds with bond lengths of 2.495(4), 2.493(4), 2.502(4), and 2.494(4) Å, respectively (Table S2†). Thus, the coordination environments of U1 and U2 show a near-perfect regular icosahedron (Fig. 1b). The bond lengths of Mo–O bonds are in the range of 1.692(4)–2.304(4) Å. Fe1 is coordinated with six terminus oxygen atoms (O1/O1#2/O1#4/O2/O2#2/O2#4) from two adjacent $\{UMo_{12}O_{42}\}$ units with the bond length of 2.093(4) and 2.071(4) Å, respectively. Particularly, Ni1 in **NiUMo** only has an occupancy of 0.576 calculated by single-crystal analysis, which may be due to the difference in the synthesis procedure.

For comparison, both Fe1 in **FeUMo** and Co1 in **CoUMo** have 100% occupancy. Thus, the crystallographic $\{NiUMo_{12}\}_n$ 1D chains are incomplete and have defects compared with $\{FeUMo_{12}\}_n$ and $\{CoUMo_{12}\}_n$. The valences of U1, U2, Mo1–Mo4, and Fe1 (Co1/Ni1) are confirmed by bond valence sum (BVS) calculation (Table S3†). Na1 and Na2 ions are coordinated by three terminal oxygen atoms from one $\{UMo_{12}O_{42}\}$ unit and three water molecules. Thus, one $\{UMo_{12}O_{42}\}$ unit is coordinated by two Fe^{II} ions and six Na ions (Fig. 1c). Adjacent $\{UMo_{12}O_{42}\}$ units are alternately connected by Fe^{II} ions to form a $\{FeUMo_{12}\}_n$ 1D chain (Fig. 1d). The adjacent Na ions are connected by bridging water molecules (O16/O16A) to form a rhombic tetranuclear Na–H_2O cluster (Fig. 1e). One tetranuclear Na–H_2O cluster then connects with four adjacent equivalent tetranuclear Na–H_2O clusters *via* bridging water molecules (O17/O17A). The 1D chain of $\{FeUMo_{12}\}_n$ is then extended by the connection of Na ions and bridging water molecules to form the 3D packing structures of **FeUMo** (Fig. 2a). It is interesting to find that the $\{FeUMo_{12}\}_n$ 1D chains in **FeUMo** have four directions in space (Fig. 2b). The space perspective angle is along a 1D chain, the projections of six adjacent overlapped 1D chains could form a regular hexagon configuration on the paper plane that matches the highly symmetrical $Ia\bar{3}$ space group perfectly. The central 1D chain that is perpendicular to the paper plane is just located at the symcenter of this regular hexagon.

In addition, FT-IR and Raman spectra revealed the characteristic vibrations of the Mo–O and Mo=O bands of **FeUMo**, **CoUMo**, and **NiUMo** (Fig. S5 and S6†). Their thermostabilities were evaluated by TGA, which indicates that the frameworks of these compounds could remain stable at temperatures below 400 °C (Fig. S7†). The impurities and chemical composition of the prepared samples were confirmed by PXRD, EDS, and XPS,

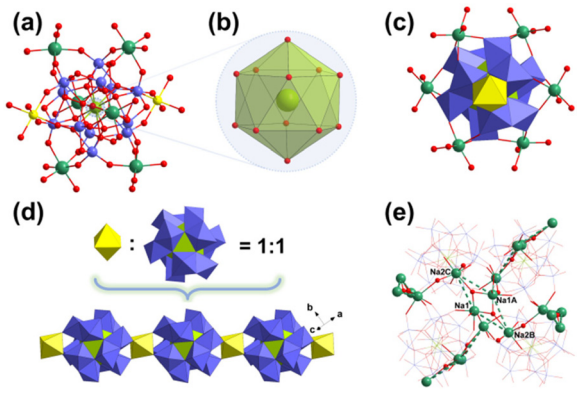

Fig. 1 (a) Ball-and-stick view of the $\{FeUMo_{12}\}$ unit; (b) the coordination environment of U1; (c) the six disordered Na ions coordinated with one center $\{FeUMo_{12}\}$ unit; (d) schematic diagram of the $\{FeUMo_{12}\}_n$ 1D chain; (e) the connection modes of the tetranuclear Na–H_2O clusters. Color codes: Fe(II), yellow; U(IV), light green; Mo, blue; Na, green; O, red.

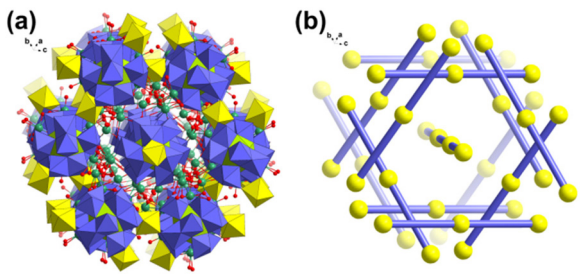

Fig. 2 (a) The 3D packing structure of **FeUMo**; (b) the simplified diagram of the 3D packing structure. Na ions and water molecules are omitted for clarity, yellow balls and blue sticks represent Fe ions and $\{UMo_{12}\}$ units, respectively.

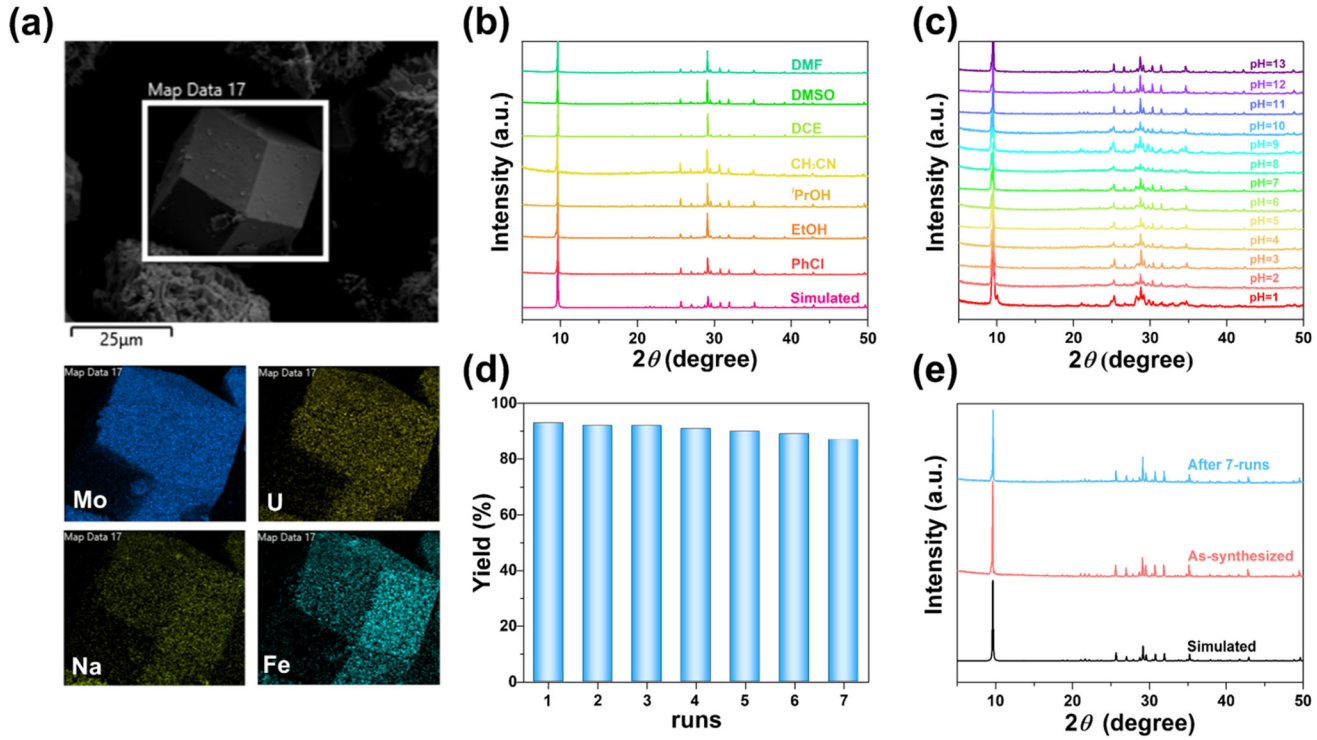

Fig. 3 (a) The EDS mapping of metal elements in **FeUMo**; (b) the PXRD patterns of **NiUMo** after being heated in different organic solvents for one day; (c) the PXRD patterns of **NiUMo** after being soaked in water solutions with different pH values for one day; (d) the cyclic yields of NiUMo; (e) **the PXRD** patterns of **NiUMo** after 7-cycles catalytic reactions.

respectively (Fig. 3a, S8–S16†). To evaluate the stability of **NiUMo**, the samples were soaked in water solutions of different pH values from 1 to 13 at room temperature and different organic solvents at 90 °C for one day, respectively. As shown in Fig. 3b and c, no significant change in the PXRD of **NiUMo** under all these conditions was observed, indicating high stability. To the best of our knowledge, the applications of crystalline materials are always limited by their stabilities. Generally, those organic–inorganic hybrid POMs obtained by hydrothermal method usually have good stability, and it is quite rare to find pure inorganic POMs with such good stability in various solvents. The outstanding stability of **NiUMo** may be attributed to the strong coordination bonds and the closely-packed 3D structure formed under hydrothermal conditions, which may be conducive to the performance of **NiUMo** as a heterogeneous catalyst for organic synthesis.

Evaluation of the catalytic activities

The Lewis acidity of a catalyst is of significant importance for catalytic performances.[37–39] Thus, we evaluated the heterogeneous Lewis acid catalytic properties of **FeUMo**, **CoUMo**, and **NiUMo** in the acetalization of 2-aminobenzamides with aldehydes, which is a highly effective method for the synthesis of 2,3-dihydroquinazolinone (DHQZ). As a privileged nitrogen-containing six-membered heterocyclic scaffold, the DHQZ family of compounds is important for pharmacological activities, such as anti-biotics, anti-fibrillation, vasodilation, and analgesia.[40,41]

After screening and optimization of a series of reaction conditions, including catalyst, solvent, temperature, time, and loading of catalyst (Tables S4–S8†), we realized that **NiUMo** was the best active catalyst among the three titled compounds for the condensation and cyclization of 2-aminobenzamide with benzaldehyde. Loading 3 mol% **NiUMo** catalyzed the condensation/amine addition of 2-aminobenzamide with benzaldehyde to generate the desired product with a yield of 93% in CH_3CN at 90 °C for 2 h. There was only a small amount of unreacted raw material under the optimal conditions, apart from the desired product **3a** and the by-product (water), which indicated the environmentally friendliness of the reaction. In addition, the reusability of **NiUMo** was investigated using 2-aminobenzamide and benzaldehyde as model substrates. After the reaction, **NiUMo** could be filtered from the reaction mixture, and could be used at least 7 times without significant loss in activity (Fig. 3d). The cycle test proved the heterogeneous nature of this catalytic system. The PXRD and FTIR pattern of the recovered **NiUMo** after catalytic reactions revealed its stability (Fig. 3e and S17†). The hot filtration experiment showed that the yield of the desired product remains nearly constant after separating the catalyst, which proved the heterogeneous nature of this catalytic system (Fig. S18†). The aforementioned results demonstrate that the

Table 1 Acetalization of 2-aminobenzamides and aldehydes[a]

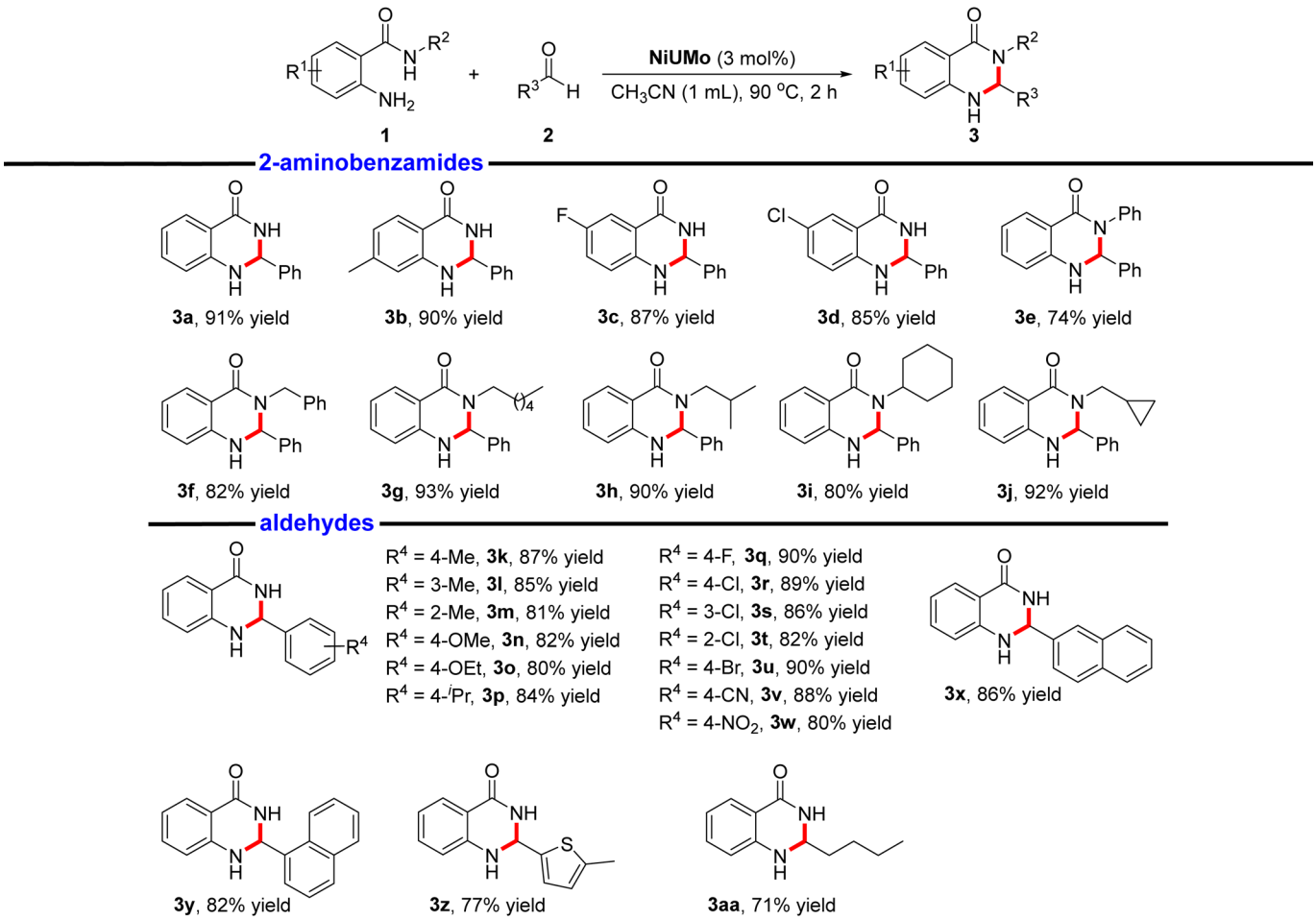

[a] Reaction conditions: 2-aminobenzamides **1** (0.2 mmol), aldehydes **2** (0.2 mmol), **NiUMo** (3 mol%), CH_3CN (1 mL), 90 °C, 2 h; isolated yield.

catalyst remains unchanged throughout the entire reaction process, and no additional hazardous components have been introduced into the reaction system.

The optimized conditions were then applied to a variety of 2-aminobenzamides with aldehydes (Table 1). Electron-donating or withdrawing groups were well-tolerated on the 2-aminobenzamides, and the corresponding DHQZ products **3a–3d** were isolated in good yields (up to 91%). However, the yields of their corresponding products are significantly lower than those of the aliphatic chain-containing due to the large potential barrier effect of the benzene ring and cyclohexane. However, for 2-amino-*N*-phenylbenzamide, 2-amino-*N*-benzylbenzamide, and 2-amino-*N*-cyclohexylbenzamide, the yield of their corresponding products is significantly lower than that of the desired products produced by the reaction of 2-amino-*N*-hexylbenzamide, 2-amino-*N*-isobutylbenzamide and 2-amino-*N*-(cyclopropylmethyl)benzamide containing aliphatic chains with benzaldehyde due to the large potential barrier effect of the benzene ring and cyclohexane (**3e–3j**). In addition, it was shown that benzaldehydes bearing electron-withdrawing groups with 2-aminobenzamide afforded the DHQZ products with higher yields than the ones with electron-rich substituents (**3k–3w**). The possible reason is that the existence of electron-withdrawing groups on the benzene ring leads to the enhancement of the electrophilic activity of the aldehyde group. 2-Naphthaldehyde and 1-naphthaldehyde underwent the condensation/amine addition with 2-aminobenzamide in excellent yields. Similarly, the spatial resistance of 2-naphthaldehyde leads to its better reactivity than 1-naphthaldehyde to obtain the desired products in higher yields (**3x** and **3y**). Subsequently, we applied the optimal conditions to the reaction of the five-membered heterocyclic aldehyde 5-methylthiophene-2-carbaldehyde, and obtained the corresponding product in 77% yield (**3z**). This yield is significantly lower than the yields of the products obtained after the above reaction of aldehydes. Meanwhile, under standard conditions, pentanal reacted with 2-aminobenzamide with a yield of 71% (**3aa**). The unprotected N–H bonds and carbonyl groups that exist in the product skeletons provide the potential for further functionalization, which opens the possibility for the development of new drugs containing quinazolinone scaffolds.

Investigation of reaction mechanism

To investigate the reaction mechanism, a series of control experiments were conducted (Fig. 4a and Table S9†).

Compared with the blank experiment without a catalyst, $NiSO_4{\cdot}7H_2O$ exhibited certain catalytic activities in the acetalization reaction of 2-aminobenzamide and aldehyde, but was lower than the **NiUMo** under standard conditions. Moreover, a Na salt of $[UMo_{12}O_{42}]^{8-}$, $Na_{5.8}H_{2.2}[UMo_{12}O_{42}]{\cdot}13.5H_2O$ (**NaUMo**), was synthesized under a similar condition. **NaUMo** had a similar structure to the titled compounds (Fig. S4†), and showed some catalytic activity for this reaction. However, it was lower than that of $NiSO_4{\cdot}7H_2O$. In addition, the catalytic activity of a mixture of $NiSO_4{\cdot}7H_2O$ and **NaUMo** is higher than either of them alone, but lower than that of **NiUMo**. These results implied that the fully exposed [Ni] in **NiUMo** acts as the Lewis acid active site to catalyze the acetalization reaction, and there is a synergistic interaction between nickel and $\{UMo_{12}O_{42}\}$. In addition, when the aldimine was used as substrate, the corresponding product was obtained in 94% yield, suggesting that aldimine was the key intermediate for this acetalization reaction. To further understand the catalytic process of the POMs, we monitored the dynamic process in the synthesis of 2-phenyl-2,3-DHQZ by **NiUMo**. As shown in Fig. 4b, with the presence of **NiUMo**, about 40% of benzaldehyde was converted to the aldimine intermediate within the first 5 min, and 9% of the desired product was detected. As the reaction progresses, the yield of the desired product increases along with the consumption of aldimine intermediates and benzaldehyde. Finally, the reaction ends with the disappearance of benzaldehyde.

Based on the above results and related literature,[42,43] the following catalytic reaction mechanism is proposed. As shown in Fig. 5, the Lewis acid active sites of [Ni] in **NiUMo** can coordinate with the oxygen atom of aldehydes, which will facilitate the nucleophilic attack by the nitrogen on the carbon of the carbonyl group to form a hydroxyl intermediate. Furthermore, the oxygen-rich surface of $\{UMo_{12}O_{42}\}$ may enrich 2-aminobenzamides through the formation of hydrogen bonds (N–H···O), resulting in a positive interaction with aldehydes. After that, the catalyst stimulates the construction of the aldimine intermediate by eliminating a water molecule. The activation of imines with the catalyst facilitates intramolecular cyclization, resulting in the formation of the desired dihydroquinazolin-4(1*H*)-one derivatives.

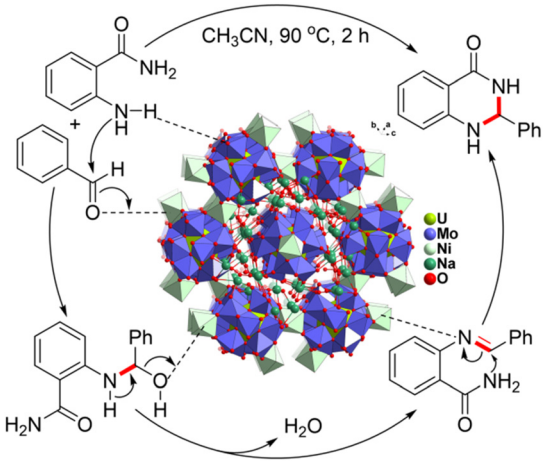

Fig. 5 The possible mechanism for the acetalization reaction of 2-aminobenzamide and aldehyde catalyzed by **NiUMo**.

Conclusions

In summary, we successfully designed and synthesized three Silverton-type multidimensional U-POMs, (**FeUMo**, **CoUMo**, and **NiUMo**), which were the first series of U-POMs with U^{IV} as a heteroatom and linked by Fe^{II}, Co^{II}, and Ni^{II}. The success of these compounds provides a reference for the adsorption, immobilization, recycling, and reuse of uranium through the hydrothermal construction of POMs. These highly stable compounds show excellent Lewis catalytic activity for the synthesis

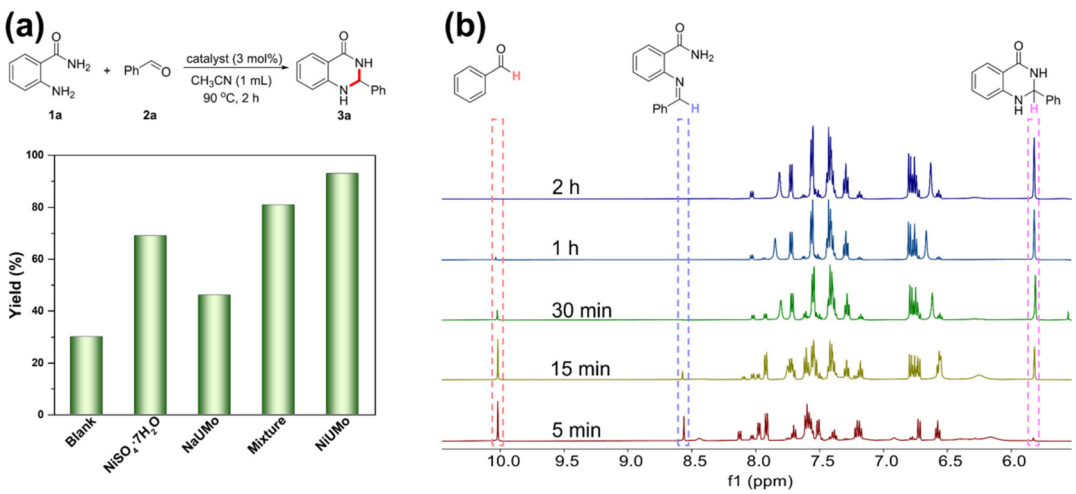

Fig. 4 (a) Control experiments; (b) evolution of ^{1}H NMR spectra during the reaction for the synthesis of 2-phenyl-2,3-DHQZ by **NiUMo**.

of quinazolinone drug precursor skeletons with water as the sole by-product. Meanwhile, **NiUMo** has excellent universality for different types of substrates, and can be recycled multiple times without deterioration of catalytic activity. This work may inspire the research about storage and reuse of actinide elements, and provide an efficient catalytic system for the synthesis of quinazolinones in a green manner.

Author contributions

Conceptualization: K. L., Y. F. L., G. P. Y., and Y. G. W.; catalyst preparation and characterization, and undertaking of related experiments: K. L. and Y. F. L.; formal analysis: K. L., Y. F. L., and G. P. Y.; writing: K. L., Y. F. L., Z. J. Z., X. L. L., and S. J. L.; supervision: G. P. Y., Y. H. L., and Y. G. W.

Conflicts of interest

There are no conflicts to declare.

Acknowledgements

The authors acknowledge the financial support from the National Natural Science Foundation of China (22001034, 22301034).

References

1 J. J. Cao, A. Cohen, J. Hansen, R. Lester, P. Peterson and H. J. Xu, *Science*, 2016, **353**, 547–548.
2 G. H. Marcus, *Nat. Rev. Phys.*, 2019, **1**, 172–173.
3 Q. Wang, R. Li and G. He, *Renewable Sustainable Energy Rev.*, 2018, **90**, 90–96.
4 L. Flett, C. L. McLeod, J. L. McCarty, B. J. Shaulis, J. J. Fain and M. P. S. Krekeler, *Environ. Res.*, 2021, **194**, 110619.
5 Z. Y. Wang, Q. H. Meng, R. C. Ma, Z. K. Wang, Y. J. Yang, H. Y. Sha, X. J. Ma, X. H. Ruan, X. Q. Zou, Y. Yuan and G. S. Zhu, *Chem*, 2020, **6**, 1683–1691.
6 C. R. Armstrong, M. Nyman, T. Shvareva, G. E. Sigmon, P. C. Burns and A. Navrotsky, *Proc. Natl. Acad. Sci. U. S. A.*, 2012, **109**, 1874–1877.
7 I. Colliard, G. Morrison, H.-C. z. Loye and M. Nyman, *J. Am. Chem. Soc.*, 2020, **142**, 9039–9047.
8 K. E. Knope and L. Soderholm, *Chem. Rev.*, 2013, **113**, 944–994.
9 K. J. Pastoor, R. S. Kemp, M. P. Jensen and J. C. Shafer, *Inorg. Chem.*, 2021, **60**, 8347–8367.
10 Y. M. Ren, H. L. Bao, Q. Wu, H. S. Wang, T. Gai, L. Shao, S. F. Wang, H. Tang, Y. R. Li and X. K. Wang, *Materials*, 2020, **391**, 122207.
11 X. Q. Xin, I. Douair, T. Rajeshkumar, Y. Zhao, S. A. Wang, L. Maron and C. Q. Zhu, *Nat. Commun.*, 2022, **13**, 3809.
12 D. E. Felton, M. Fairley, A. Arteaga, M. Nyman, J. A. LaVerne and P. C. Burns, *Inorg. Chem.*, 2022, **61**, 11916–11922.
13 Q. Hu, S. Chen, T. Wågberg, H. Zhou, S. Li, Y. Li, Y. Tan, W. Hu, Y. Ding and X. B. Han, *Angew. Chem., Int. Ed.*, 2023, **62**, e202303290.
14 Q. D. Liu and X. Wang, Polyoxometalate Clusters: Sub-Nanometer Building Blocks for Construction of Advanced Materials, *Matter*, 2020, **2**, 816–841.
15 Y. F. Liu, C. W. Hu and G. P. Yang, *Chin. Chem. Lett.*, 2023, **34**, 108097.
16 Y. B. Ma, F. Gao, W. R. Xiao, N. Li, S. J. Li, B. Yu and X. N. Chen, *Chin. Chem. Lett.*, 2022, **33**, 4395–4399.
17 Z. Y. Tian, X. Q. Han, J. Du, Z. B. Li, Y. Y. Ma and Z. G. Han, *ACS Appl. Mater. Interfaces*, 2023, **15**, 11853–11865.
18 Z. Zeb, Y. C. Huang, L. L. Chen, W. B. Zhou, M. H. Liao, Y. Y. Jiang, H. T. Li, L. Wang, L. M. Wang, H. Wang, T. Wei, D. J. Zang, Z. J. Fan and Y. G. Wei, *Coord. Chem. Rev.*, 2023, **482**, 215058.
19 M. Dufaye, S. Duval and T. Loiseau, *CrystEngComm*, 2020, **22**, 3549–3562.
20 K.-C. Kim and M. T. Pope, *J. Am. Chem. Soc.*, 1999, **121**, 8512–8517.
21 G. P. Yang, K. Li and C. W. Hu, *Inorg. Chem. Front.*, 2022, **9**, 5408–5433.
22 H. L. Zhang, A. Li, K. Li, Z. P. Wang, X. C. Xu, Y. X. Wang, M. V. Sheridan, H. S. Hu, C. Xu, E. V. Alekseev, Z. Y. Zhang, P. Yan, K. C. Cao, Z. F. Chai, T. E. Albrecht-Schönzart and S. A. Wang, *Nature*, 2023, **616**, 482–487.
23 H. L. Zhang, W. Liu, A. Li, D. Zhang, X. Y. Li, F. W. Zhai, L. H. Chen, L. Chen, Y. L. Wang and S. A. Wang, *Angew. Chem., Int. Ed.*, 2019, **58**, 16110–16114.
24 P. Baidala, V. S. Smurova, E. A. Torchenkova and V. I. Spitsyn, *Dokl. Chem.*, 1971, **197**, 202.
25 T. Auvray and E. M. Matson, *Dalton Trans.*, 2020, **49**, 13917–13927.
26 Y. F. Liu, K. Li, H. Y. Lian, X. J. Chen, X. L. Zhang and G. P. Yang, *Inorg. Chem.*, 2022, **61**, 20358–20364.
27 V. N. Molchanov, I. V. Tatjanina, E. A. Torchenkova and L. P. Kazansky, *J. Chem. Soc., Chem. Commun.*, 1981, 93–94.
28 M. T. Pope, *Structural Chemistry of Inorganic Actinide Compounds*, Elsevier, 2007, ch. 9, pp. 341–361.
29 M. A. Petrukhina, V. N. Molchanov, I. V. Tat'yanina and E. A. Torchenkova, *Kristallografiya*, 1990, **35**, 386–389.
30 M. A. Petrukhina, V. S. Sergienko, G. G. Sadikov, I. V. Tat'yanina and E. A. Torchenkova, *Koord. Khim.*, 1990, **16**, 354–360.
31 E. P. Samokhvalova, V. N. Molchanov, I. V. Tat'yanina and E. A. Torchenkova, *Koord. Khim.*, 1990, **16**, 207–211.
32 E. P. Samokhvalova, V. N. Molchanov, I. V. Tat'yanina and E. A. Torchenkova, *Koord. Khim.*, 1990, **16**, 1277–1282.
33 I. V. Tat'yanina, E. B. Fomicheva, V. N. Molchanov, V. E. Zavodnik, V. K. Bel'skij and E. A. Torchenkova, *Kristallografiya*, 1982, **27**, 233–238.

34 M. K. Kotvanova, V. N. Molchanov, E. A. Torchenkova and V. I. Spitsyn, *Zh. Neorg. Khim.*, 1984, **29**, 1790–1797.
35 M. K. Kotvanova, V. N. Molchanov, E. A. Torchenkova and K. I. Kim, *Koord. Khim.*, 1984, **10**, 993–997.
36 Y. Y. Dong, Z. M. Dong, Z. B. Zhang, Y. H. Liu, W. W. Cheng, H. Miao, X. X. He and Y. Xu, *ACS Appl. Mater. Interfaces*, 2017, **9**, 22088–22092.
37 K. Li, Y. F. Liu, X. L. Lin and G. P. Yang, *Inorg. Chem.*, 2022, **61**, 6934–6942.
38 X. R. Tian, Z. Y. Jiang, S. L. Hou, H. S. Hu, J. Li and B. Zhao, *Angew. Chem., Int. Ed.*, 2023, **62**, e202301764.
39 G. P. Yang, X. L. Zhang, Y. F. Liu, D. D. Zhang, K. Li and C. W. Hu, *Inorg. Chem. Front.*, 2021, **8**, 4650–4656.
40 G. M. Chinigo, M. Paige, S. Grindrod, E. Hamel, S. Dakshanamurthy, M. Chruszcz, W. Minor and M. L. Brown, *J. Med. Chem.*, 2008, **51**, 4620–4631.
41 J. Wu, X. L. Du, J. Ma, Y. P. Zhang, Q. C. Shi, L. J. Luo, B. A. Song, S. Yang and D. Y. Hu, *Green Chem.*, 2014, **16**, 3210–3217.
42 J. J. Jiao, Z. J. Li, Z. W. Qiao, X. Li, Y. Liu, J. Q. Dong, J. W. Jiang and Y. Cui, *Nat. Commun.*, 2018, **9**, 4423.
43 G. Kumar, N. K. Mogha and D. T. Masram, *ACS Appl. Nano Mater.*, 2021, **4**, 2682–2693.